Seasonal stratification, shell flux, and oxygen isotope dynamics of left-coiling *N. pachyderma* and *T. quinqueloba* in the western subpolar North Atlantic

Lukas Jonkers,[1] Geert-Jan A. Brummer,[1] Frank J. C. Peeters,[2] Hendrik M. van Aken,[3] and M. Femke De Jong[3]

Received 17 August 2009; revised 21 November 2009; accepted 15 December 2009; published 6 May 2010.

[1] We present an almost 3 year long time series of shell fluxes and oxygen isotopes of left-coiling *Neogloboquadrina pachyderma* and *Turborotalita quinqueloba* from sediment traps moored in the deep central Irminger Sea. We determined their response to the seasonal change from a deeply mixed water column with occasional deep convection in winter to a thermally stratified water column with a surface mixed layer (SML) of around 50 m in summer. Both species display very low fluxes during winter with a remnant summer population holding out until replaced by a vital population that seeds the subsequent blooms. This annual population overturning is marked by a 0.7‰ increase in $\delta^{18}O$ in both species. The shell flux of *N. pachyderma* peaks during the spring bloom and in late summer, when stratification is close to its minimum and maximum, respectively. Both export periods contribute about equally and account for >95% of the total annual flux. Shell fluxes of *T. quinqueloba* show only a single broad pulse in summer, thus following the seasonal stratification cycle. The $\delta^{18}O$ of *N. pachyderma* reflects temperatures just below the base of the seasonal SML without offset from isotopic equilibrium. The $\delta^{18}O$ pattern of *T. quinqueloba* shows a nearly identical amplitude and correlates highly with the $\delta^{18}O$ of *N. pachyderma*. Therefore *T. quinqueloba* also reflects temperature near the base of the SML but with a positive offset from isotopic equilibrium. These offsets contrast with observations elsewhere and suggest a variable offset from equilibrium calcification for both species. In the Irminger Sea the species consistently show a contrast in their flux timings. Their flux-weighted $\Delta\delta^{18}O$ will thus dominantly be determined by seasonal temperature differences at the base of the SML rather than by differences in their depth habitat. Consequently, their sedimentary $\Delta\delta^{18}O$ may be used to infer the seasonal contrast in temperature at the base of the SML.

Citation: Jonkers, L., G.-J. A. Brummer, F. J. C. Peeters, H. M. van Aken, and M. F. De Jong (2010), Seasonal stratification, shell flux, and oxygen isotope dynamics of left-coiling *N. pachyderma* and *T. quinqueloba* in the western subpolar North Atlantic, *Paleoceanography*, *25*, PA2204, doi:10.1029/2009PA001849.

1. Introduction

[2] The oxygen isotope signature of planktonic foraminifera has long been successfully applied to reconstruct past continental ice volumes and sea surface conditions from sediment cores [e.g., *Shackleton*, 1967]. In-depth knowledge on when and at what depth planktonic foraminifera register the oxygen isotope signature of the ambient water is not only a prerequisite for paleoceanographic inferences, but may additionally carry reconstructions beyond conventional estimates of mean conditions toward addressing past upper ocean seasonal variability. Given depth habitat differences between species, their interspecies $\Delta\delta^{18}O$ can be used to trace past stratification of the upper ocean [*Mulitza et al.*, 1997; *Rashid and Boyle*, 2007; *Simstich et al.*, 2003]. Seasonal differences in growing periods may however result in similar sedimentary $\Delta\delta^{18}O$ and bias paleoceanographic inferences of stratification [e.g., *Conan and Brummer*, 2000; *Deuser and Ross*, 1989; *Hillaire-Marcel and de Vernal*, 2008]. It is therefore essential to constrain both the vertical and seasonal distribution of planktonic foraminifera whose oxygen isotope composition is used to infer past ocean dynamics.

[3] Here we report on an almost 3 year long record of intercepted sediment fluxes from the central Irminger Sea. We concentrate on *Neogloboquadrina pachyderma* (the sinistral coiled species as opposed to the dextral *N. incompta*) and *Turborotalita quinqueloba* as together they account for over half of the total planktonic foraminiferal shell flux during the main export season. Both species are found abundantly in the sedimentary record [e.g., *Carstens et al.*, 1997; *Pflaumann et al.*, 1996; *Schröder-Ritzrau et al.*, 2001] and often used to infer past oceanography [e.g., *Aksu et al.*,

[1]Department of Marine Geology, Royal Netherlands Institute for Sea Research, Den Burg, Netherlands.
[2]Section Marine Biogeology, Faculty of Earth and Life Sciences, Vrije University Amsterdam, Amsterdam, Netherlands.
[3]Department of Physical Oceanography, Royal Netherlands Institute for Sea Research, Den Burg, Netherlands.

0883-8305/10/2009PA001849

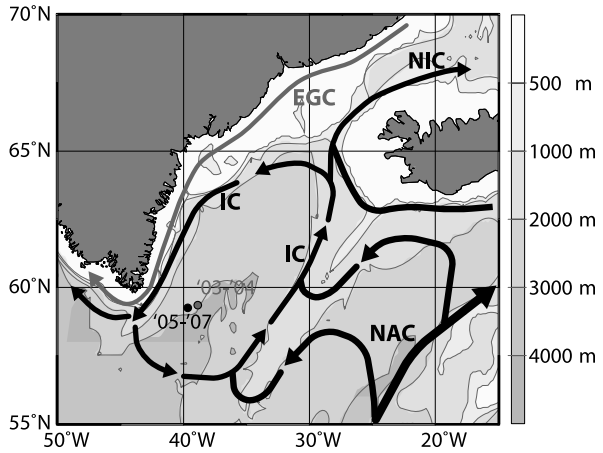

Figure 1. Schematic surface hydrography of the western North Atlantic and locations of moored sediment traps [*Nansen*, 1912]. Black lines indicate warm surface currents, North Atlantic Current (NAC), Irminger Current (IC), and North Iceland Irminger Current (NIC), and the Irminger Gyre. The gray line depicts the cold East Greenland Current (EGC). Moorings (IRM-1, 3, and 4) are indicated by dots.

2002; *Castañeda et al.*, 2004; *Kahn et al.*, 1981; *Nørgaard-Pedersen et al.*, 2007; *van Kreveld et al.*, 2000]. Additionally, the species oxygen isotopic difference has been proposed as an indicator of thermal stratification [*Simstich et al.*, 2003] and our data set allows for evaluating this proposed method in the North Atlantic. The left coiling (morpho)species *N. pachyderma* [*Cifelli*, 1973; *Darling et al.*, 2006] is a (sub)polar species that dominates in cold areas, where it constitutes almost 100% of the total foraminiferal fauna found in sediments [*Bé and Tolderlund*, 1971; *Schröder-Ritzrau et al.*, 2001]. The species thrives at temperatures below 10°C [*Bé and Tolderlund*, 1971; *Tolderlund and Bé*, 1971]. Individuals are found throughout the upper water column, generally most abundantly in the upper 50 to 100 m, but most calcification is reported to occur at depths ranging from 100 to 200 m [*Bauch et al.*, 1997; *Simstich et al.*, 2003; *Stangeew*, 2001; *Volkmann and Mensch*, 2001].

[4] The other species of interest, *T. quinqueloba,* is generally found in warmer waters than *N. pachyderma* [*Bé and Tolderlund*, 1971], yet may dominate at high northern latitudes [*Stangeew*, 2001]. In the Nordic Seas it is associated with the western side (cold) of the Arctic front [*Schröder-Ritzrau et al.*, 2001]. According to *Hemleben et al.* [1989] the species is symbiont bearing and due to the symbionts' dependence on light for photosynthesis it is considered a (near-) surface dweller [*Bé and Tolderlund*, 1971; *Simstich et al.*, 2003]. High abundances at greater depth [*Schiebel and Hemleben*, 2000; *Stangeew*, 2001] may be introduced by the low sinking speed of its small, thin-walled test [*Schiebel and Hemleben*, 2000]. Since *T. quinqueloba* undergoes little secondary calcification at depth, its isotopic signal is thought to reflect conditions near the surface [*Simstich et al.*, 2003]. Based on depth habitat differences between *N. pachyderma* and *T. quinqueloba Simstich et al.* [2003] proposed that their $\Delta\delta^{18}O$ reflects thermal stratification of the upper water column. We document the flux and oxygen isotope patterns of *N. pachyderma* and *T. quinqueloba* in relation to seasonal hydrographic changes, assess their isotopic offset from equilibrium $\delta^{18}O$ and propose a new mechanism based on interspecies $\Delta\delta^{18}O$ to infer past stratification and seasonality.

2. Regional Hydrography

[5] The surface water masses in the central Irminger Sea east of the southern tip of Greenland (Figure 1) are characterized by the relatively warm and saline waters of the cyclonic Irminger Gyre that surround colder waters in the center of the basin. The cold and fresh waters of the East Greenland Current are confined to a narrow zone along the Greenland continental slope. At intermediate depths (~500–2000 m) Labrador Sea Water is present [*Falina et al.*, 2007; *Yashayaev et al.*, 2007].

[6] During the annual cycle sea surface salinity varies from 34.92 PSU in winter to 34.65 PSU in summer; with the slight decrease mainly due to increased net precipitation and some meltwater input. Sea surface temperature varies from ~10°C in summer to ~5°C in winter, whereas temperatures at 200 to 250 m depth (and deeper) remain relatively constant at approximately 5°C (Figures 2a and 2b). Consequently the upper water column exhibits strong temperature stratification in summer. Multiple CTD casts during late summer and early autumn, i.e., during and just after maximum stratification, show a wind-driven surface mixed layer (SML) that is about 50 m deep (Figure 2c). Highest fluorescence levels (0.45 to 1.0 mg m^{-3}) are observed within the SML. The water column is cold and virtually homogenous (down to nearly 1000 m depth) during the winter season. This lack of stratification during the winter season is one of the main preconditions for deep convection, which occurs incidentally when atmospheric and oceanic conditions allow [*Bacon et al.*, 2003; *Pickart et al.*, 2003; *Vage et al.*, 2009]. The Irminger Sea is thus characterized by pronounced (~5°C) seasonal changes in sea surface temperature (SST) and low sea surface salinity (SSS) variability (Figure 2a), allowing to determine the effects of seasonal changes in thermal stratification on foraminiferal fluxes and isotope signatures.

3. Material and Methods

[7] Export fluxes were intercepted for nearly 3 years using moored time series sediment traps at ~2750 m water depth (250 m above the seafloor) in the central Irminger Sea (Table 1) on the WOCE A1/AR7E section. Collecting cups were rotated every 19 days during the first year and every 16 days during the last two. Tilt of the traps on the mooring line was monitored every eight minutes and was on average less than 2° ($\sigma < 0.7$) with occasional short intervals of up to 6°. Mean current speeds at trap depth during September 2007 to September 2008 were ~10 cm s^{-1}, with maxima not exceeding ~40 cm s^{-1}. Consequently, mooring line motion and hydrodynamic contrasts should not have compromised trapping efficiency.

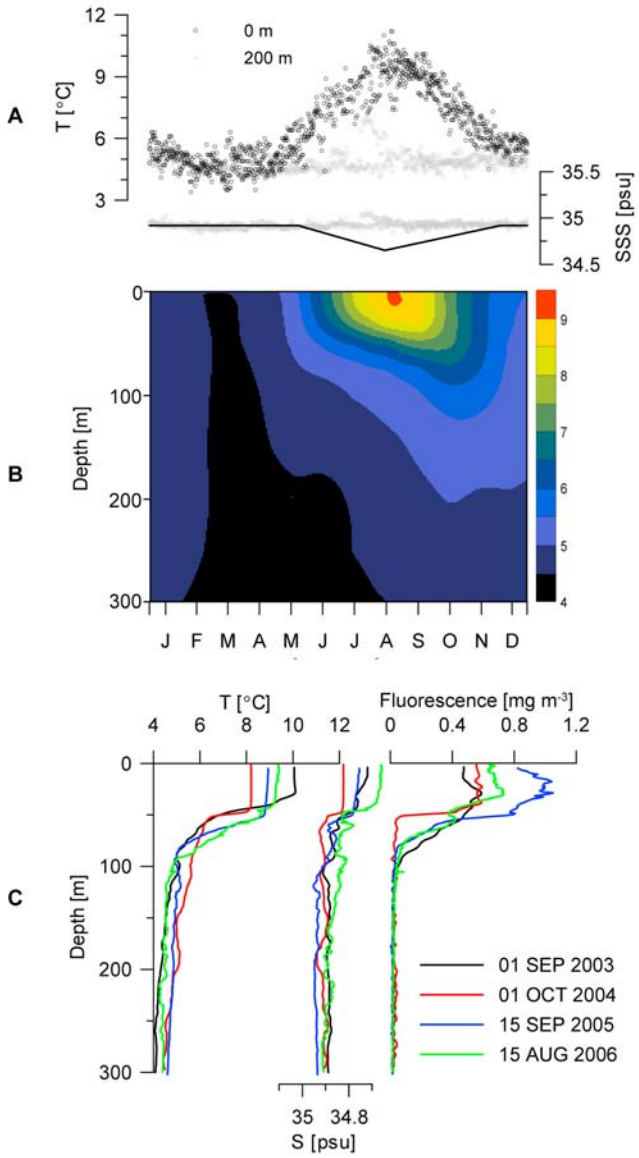

Figure 2. Annual temperature and salinity variability and autumn mixed layer depth. (a) Daily resolved temperature and salinity at the surface and at depth (black and gray symbols, respectively). (b) Contoured annual temperature down to 300 m water depth (data from WOA 2005 [*Locarnini et al.*, 2006]). (c) Temperature, salinity, and fluorescence from CTD casts conducted during mooring deployment or recovery. Note that even during maximum stratification the mixed layer does not extend deeper than ~50 m.

[8] Prior to deployment the trap bottles were filled with ambient seawater, poisoned with $HgCl_2$ (1.9 g L^{-1}) and pH buffered with Borax ($Na_2B_4O_7{\cdot}10H_2O$, 1.9 g L^{-1}). Upon recovery samples were stored at 4°C. Before sample processing the supernatant was sampled for dissolved Si analysis to enable correction for the dissolution of the particulate biogenic silica [*Bauerfeind and von Bodungen*, 2006; *Koning et al.*, 1997]. Swimmers larger than 1 mm were removed prior to splitting of the samples. One half of the samples was analyzed for total mass flux, total and organic carbon, carbonate, nitrogen and biogenic silica (BSi) content. Carbon and nitrogen were separately analyzed on weighed aliquots of the bulk material before and after removal of the carbonate carbon [*Bonnin et al.*, 2002], using a Carlo Erba Instruments Flash 1112 elemental analyzer. Biogenic silica was determined by continuous alkaline leaching that accounts for contributions by coleaching of Al silicates [*Koning et al.*, 2002].

[9] For foraminifera analysis the other half of the samples was washed using Milli-Q water over 150 and 250 μm sieves and dried at 45°C. All shells were picked from the 150 to 250 μm fraction as this is the size range normally used in paleoceanographic studies. Approximately 200 individuals (if present) were counted to determine the flux of *N. pachyderma* and *T. quinqueloba* and a rest group containing all other taxa. Stable isotopes were measured with a Finnigan MAT 253 mass spectrometer with an automated Carbo-Kiel IV preparation line. To ensure that representative samples were taken from the entire population and to assess intra population spread, six aliquots of every sample consisting of four shells were measured. Due to low shell numbers in the winter samples it was not always possible to perform multiple measurements on the same sample, yielding these observations less representative of the foraminiferal population. All isotopic values are reported versus the PDB scale established via the NBS19 carbonate stable isotope standard. Analytical precision of the standard is 0.05‰ for $\delta^{18}O$ (1 standard deviation). All raw export flux and isotope data are available in the auxiliary material.[1]

[10] Insolation values at the top of the atmosphere are based on the *Berger* [1978] solution and were downloaded from http://aom.giss.nasa.gov. Equilibrium $\delta^{18}O$ values were calculated according to *Kim and O'Neil* [1997] following the equation by *King and Howard* [2005]:

$$\delta^{18}O_{eq} = \frac{4.64 - \sqrt{21.53 - (16.1 - T)}}{0.18} + \delta^{18}O_w \qquad (1)$$

where T denotes temperature in °C and $\delta^{18}O_w$ the oxygen isotope composition of the ambient water. Temperature and salinity data were compiled from in situ measurements, real-time remote sensing and hydrographic databases. The entire water column was profiled by CTD during deployment and/or recovery of the moorings. Temperature and salinity variability below ~200 m water depth was monitored daily by an adjacent moored McLane CTD profiler (Table 1). For the 2003–2004 period the average temperature between 190 and 210 m was used, and for 2005–2007 a more continuous data set was available from the 240–260 m depth interval. Temperature differences between these depths appear negligible for this study. Satellite-derived daily sea surface temperature data (L4 AVHRR_OI) was obtained from the GODAE High Resolution Sea Surface Temperature Pilot Project (obtained from the Physical Oceanography Distributed Active Archive Center (PO.DAAC) at the NASA Jet Propulsion Laboratory, Pasadena, CA. http://podaac.jpl.

[1] Auxiliary materials are available at ftp://ftp.agu.org/apend/pa/2009pa001849.

Table 1. Details on Moored Sediment Traps

	Position	Type	Collecting Area (m^2)	Number of Bottles	Collecting Interval (days)	Start Date	CTD Profiler Position
IRM-1	59°20.74′N, 38°51.82′W	Kiel HDW	0.5	20	19	31 Aug 2003	59°25.78′N, 39°00.09′W
IRM-3	59°14.86′N, 39°39.47′W	McLane mark 78G-21	0.5	21	16	21 Sep 2005	59°16.21′N, 39°29.80′W
IRM-4	59°14.85′N, 39°39.47′W	Technicap PPS-5	1.0	17	16	5 Sep 2006	59°11.76′N, 39°30.61′W

nasa.gov). Sea surface salinity data from CTD casts was complemented by data gathered from a wider area around the site (61.5°N–57.5°N, 37.5°W–41.5°W) for the entire deployment period from the Global Temperature-Salinity Profile Program [*Operational Oceanography Group*, 2006]. Given the spatial and temporal scarcity of surface salinity data, an average sea surface salinity curve was composed (Figure 2a) and used throughout this study. Salinity variability at 200 m depth is only 0.12 PSU, of which about half is caused by a short period of increased salinity and temperature in summer 2004. Seawater $\delta^{18}O$ was estimated assuming a linear relationship between salinity and $\delta^{18}O_w$ based on regional data available through the Global Seawater Oxygen-18 Database [*Bigg and Rohling*, 2000; *Schmidt*, 1999] ($\delta^{18}O_w = 0.5417 * S - 18.767$) and subsequently converted to the PDB scale by subtracting 0.27‰ [*Hut*, 1987]. Note that the influence of varying salinity on surface equilibrium $\delta^{18}O$ is much smaller compared to that of temperature (0.27 PSU ~0.15‰ versus 7.80°C ~ 1.82‰), yielding our inferences relatively insensitive to the chosen salinity-$\delta^{18}O_w$ relationship.

[11] In order to link the deep time series fluxes and isotope changes to (near) surface processes we considered the time delay the particles need to reach the trap at 2750 m depth. *Von Gyldenfeldt et al.* [2000] reported sinking speeds for *N. pachyderma* and *T. quinqueloba* ranging from 163 to 372 m d^{-1} and 129 to 190 m d^{-1}, respectively. We shifted all *N. pachyderma* and *T. quinqueloba* records 2 and 3 weeks

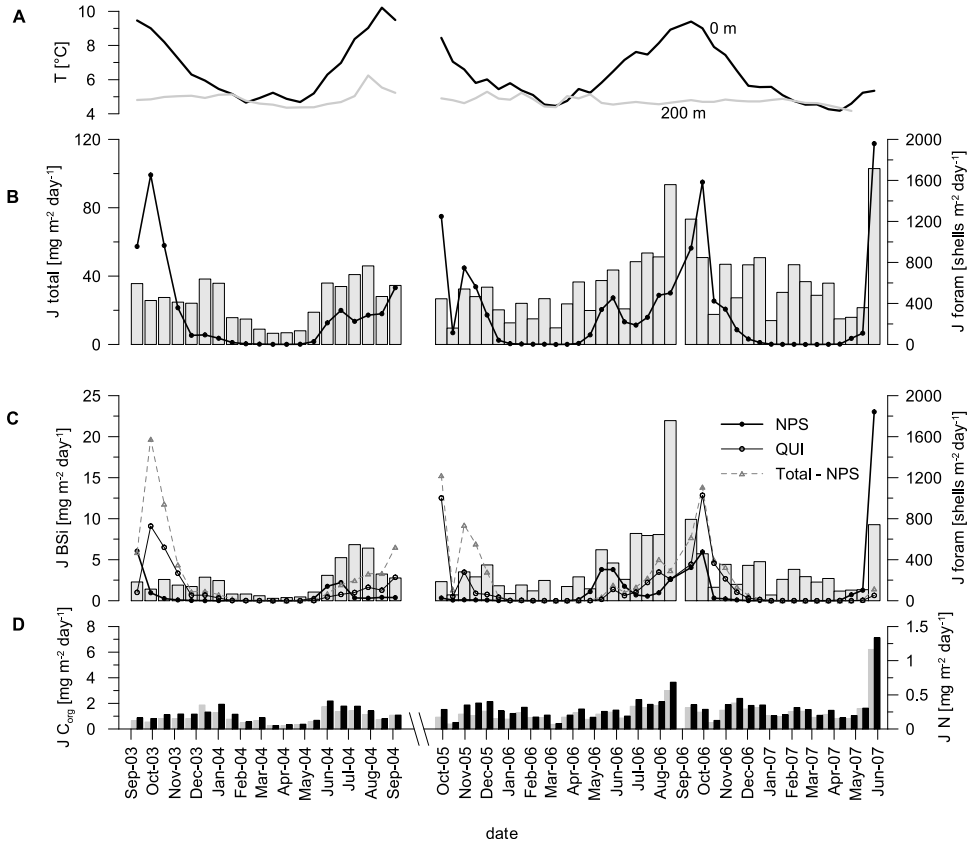

Figure 3. Intercepted fluxes (J) in relation to temperature. (a) Satellite-derived daily sea surface temperature and in situ measured temperature at 200 m depth, averaged for the collecting intervals. (b) Total mass and shell fluxes. (c) Biogenic silica (BSi) and species-specific fluxes. (d) Total N and organic carbon fluxes. Note distinct seasonality in all fluxes and that these are raw data and not compensated for settling time.

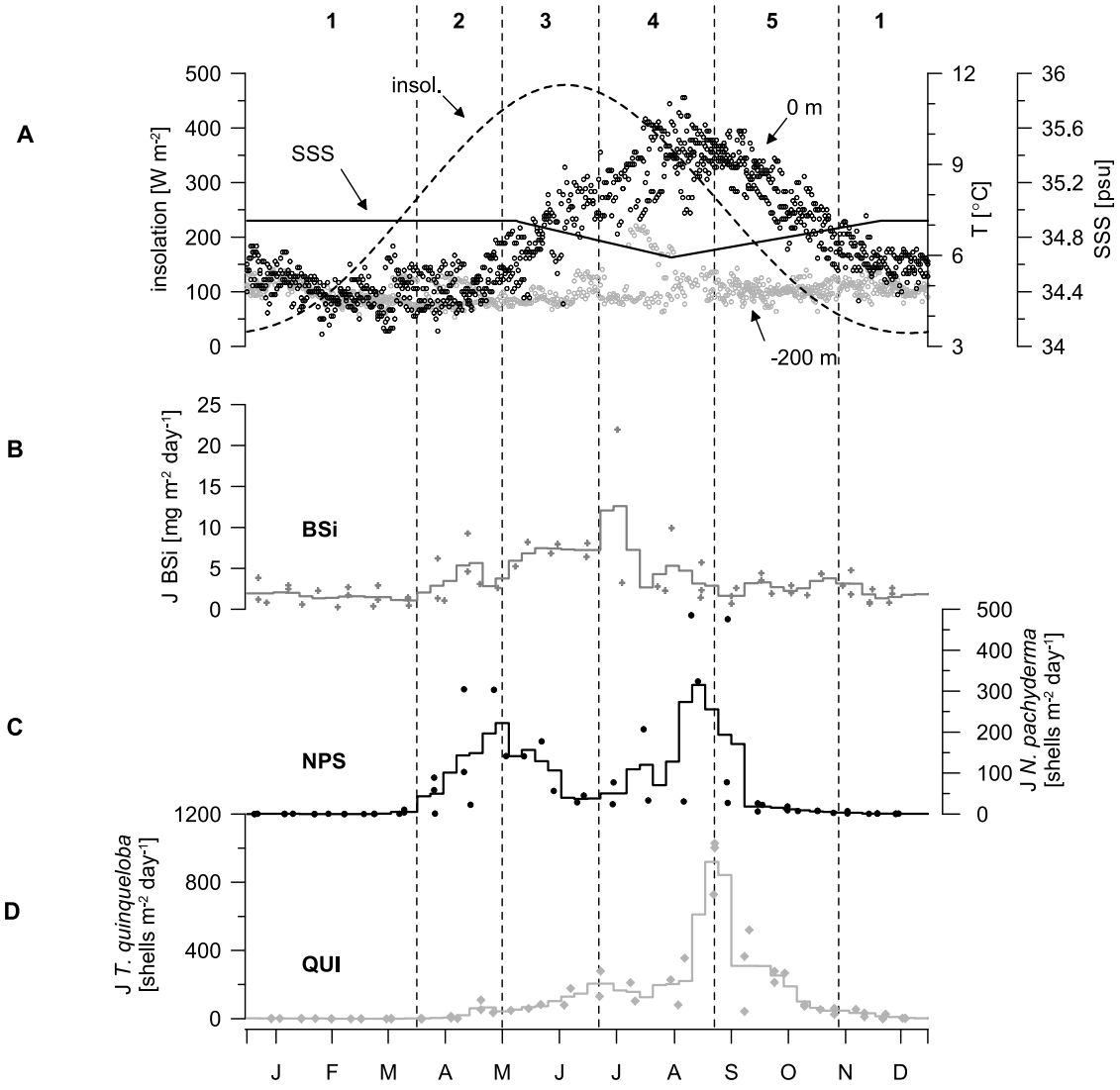

Figure 4. Stacked and time-shifted time series fluxes. (a) Annual cycles of temperature (black open circles, 0 m; gray open circles, −200 m), surface salinity (black solid line), and insolation at the top of the atmosphere (black dashed line). (b) BSi flux. (c) *N. pachyderma* flux (extremely high flux in June 2007 omitted). (d) *T. quinqueloba* flux. Vertical dashed lines separate phases (see text). In Figures 4b–4d the symbols denote the actual observations and the lines denote the weekly averaged value.

earlier, respectively, to compensate for production and settling time of the shells. Both settling times are on the high end of the velocity ranges of *Von Gyldenfeldt et al.* [2000]. This is to account for the difference between sieve and true diameter sizes, as the sieve fraction tends to be coarser and thus to settle faster. These time lags are in the same range as the temporal offset between the SST and shell $\delta^{18}O$ maxima in summer 2006, which serve as the tie point in the time series since $\delta^{18}O$ cannot lead SST. The BSi flux has been shifted back by 4 weeks to account for the lower sinking speed of the aggregates in which most BSi settles. In sections 4–6 and in Figures 4–10 this settling delay has been applied. In order to average out interannual variability, all time series records have been collapsed onto 1 year composites. This was achieved by converting all calendar dates to year days and calculation of daily averaged fluxes assuming that the observed fluxes did not vary during the 16 or 19 days collecting interval. Based on these values we derived weekly averages of different parameters and a synthetic sedimentary signal (Figures 4 and 6). Note that the symbols in Figures 4 and 6 represent the middates of the 16 to 19 days collecting intervals.

4. Results

4.1. Seasonal Fluxes

[12] Total mass fluxes intercepted at 2750 m depth vary from about 7 to 103 mg m^{-2} d^{-1} and are generally lowest in winter to early spring when the water column is mixed to great depths and highest during summer when maximum

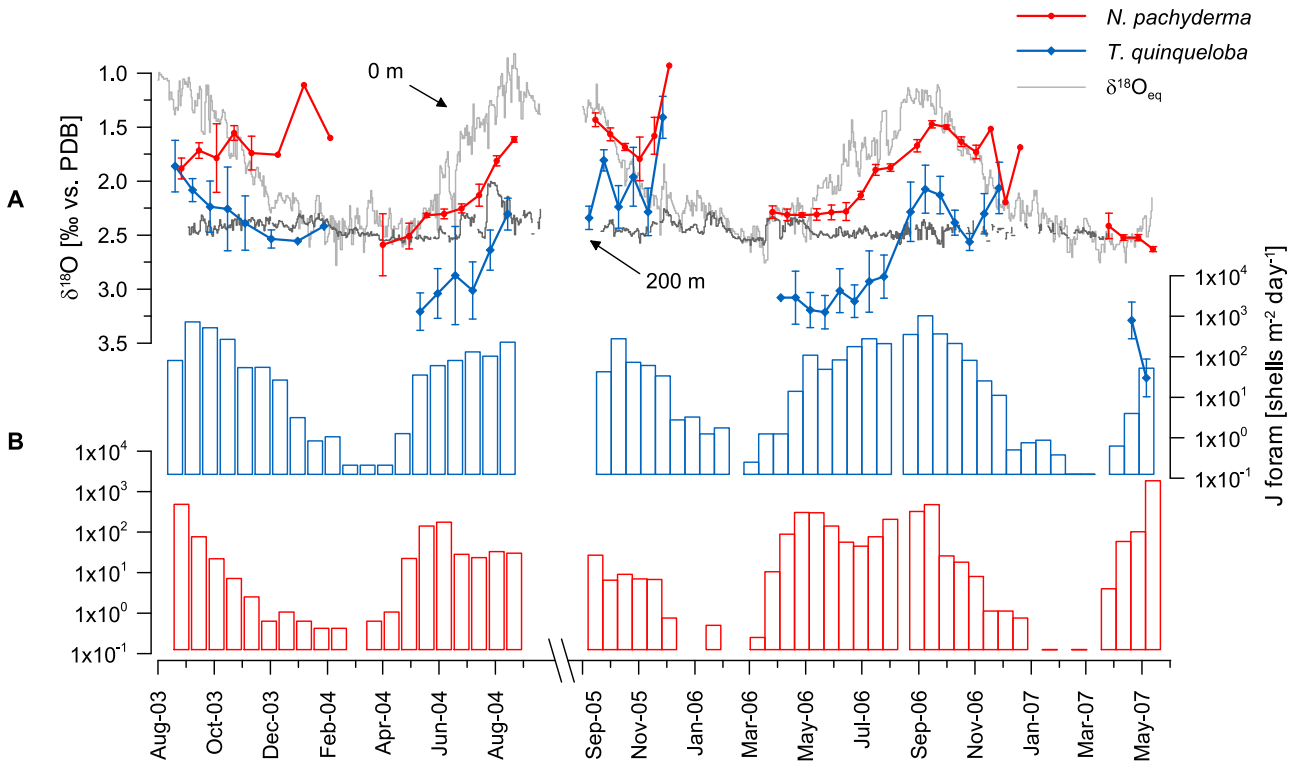

Figure 5. Time-shifted oxygen isotope patterns of *T. quinqueloba* and *N. pachyderma*. (a) Here $\delta^{18}O$ of *T. quinqueloba* and *N. pachyderma* (solid lines) with respect to $\delta^{18}O_{eq}$ (thin gray lines, calculated according to *Kim and O'Neil* [1997]) at the surface and at 200 m depth. Error bars depict standard error of replicate analyses. Samples without error bars depict measurements of single aliquots and should be taken as an indication only. Note reversed $\delta^{18}O$ axis. (b) Fluxes of *T. quinqueloba* and *N. pachyderma* plotted on a logarithmic scale.

stratification occurs (Figures 3a and 3b). As a measure of diatom export production the biogenic silica flux shows a more pronounced seasonality with low fluxes (approximately 2.5 mg m^{-2} d^{-1}) during winter and early spring (Figures 3c and 4b). The spring bloom starts in early April as evidenced by the increase in BSi fluxes, which reach maximum values of up to 22 mg m^{-2} d^{-1} in July (Figure 4b). BSi fluxes above background levels occur when insolation at the top of the atmosphere exceeds ~275 W m^{-2}. Similar to BSi, fluxes of total nitrogen and organic carbon (Figure 3d) vary from only 0.05 and 0.27 mg m^{-2} d^{-1} in winter to 1.17 and 7.13 mg m^{-2} d^{-1} in summer, respectively.

[13] Total foraminifera fluxes range over 3 orders of magnitude from near zero in winter to almost 2000 shells m^{-2} d^{-1} in summer and show two prominent pulses during the year (Figure 3b). One pulse arrives in late spring from May to June and the second in autumn, from September to November–December (Figure 3b). The spring peak in the foraminifera flux is formed almost entirely by *N. pachyderma* and its start is concurrent with the onset of the spring bloom as evidenced by an increased BSi flux (Figures 3c and 4). Shell fluxes of *N. pachyderma* remain rather low during summer, but peak again in early autumn, when stratification is at its maximum (Figures 3c and 4c). By contrast, the flux of *T. quinqueloba* shows only one broad pulse that starts to develop in spring approximately 2 to 3 weeks after *N. pachyderma* (Figure 4). Its maximum is reached in late September around SST maximum and lasts longer than that of *N. pachyderma* into December (Figure 4).

[14] The seasonal succession of settling particles can be categorized in five intergrading phases (Figure 4) of which the exact timings will differ somewhat from year to year.

[15] 1. In November–March, there is no stratification and almost zero or background fluxes of all biogenic particles. Deep convection occasionally takes place during this period [*Bacon et al.*, 2003; *Pickart et al.*, 2003; *Vage et al.*, 2009], but shell fluxes contribute very little to the total annual flux.

[16] 2. In April-mid-May, the deep winter mixed layer starts to disappear and some stratification develops; occasionally the flux of *N. pachyderma* increases to a maximum of around 200 shells m^{-2} d^{-1} in mid-May. The BSi flux increases simultaneously with that of *N. pachyderma*.

[17] 3. In mid-May–July, the SST rises, reflecting that stratification starts to increase rapidly. The shell flux of *N. pachyderma* decreases to <40 shells m^{-2} d^{-1}, while those of other species, including *T. quinqueloba*, start to increase.

[18] 4. In July-mid-September, the stratification reaches its maximum after the maximum insolation, just before the storm season starts. The flux of *T. quinqueloba* reaches its maximum at ~900 shells m^{-2} d^{-1} and *N. pachyderma* develops a second maximum around 300 shells m^{-2} d^{-1}. Both species peak around SST maximum when stratification

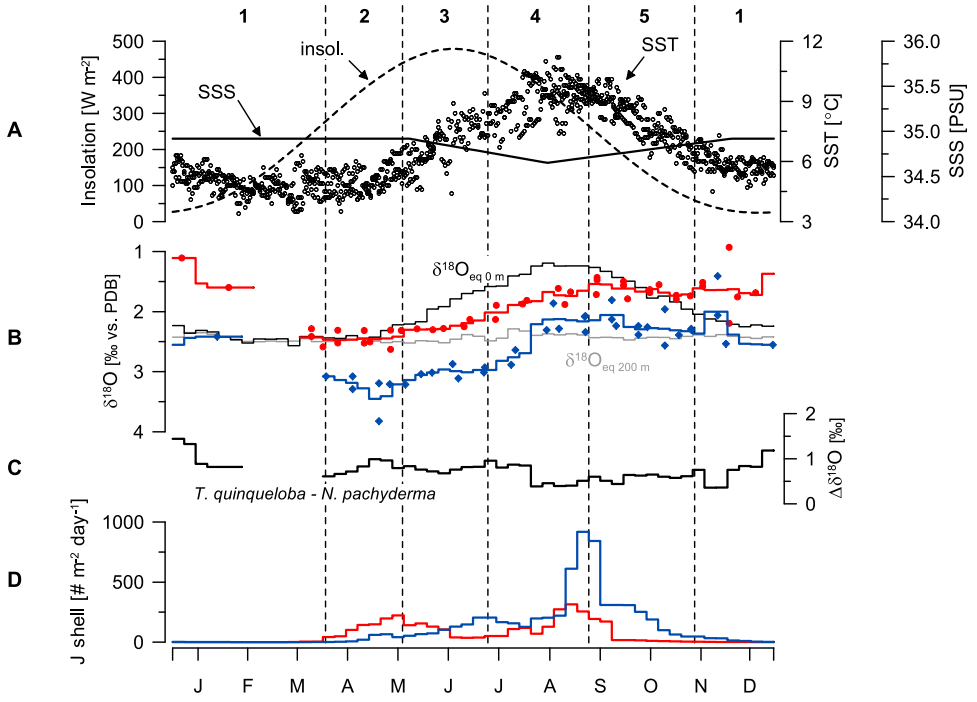

Figure 6. Stacked and time-shifted time series $\delta^{18}O$ with respect to surface $\delta^{18}O_{eq}$. Symbols indicate observed values plotted at middates of the intervals; lines are weekly averages. Thin black and gray lines show weekly $\delta^{18}O_{eq}$ at the surface and at 200 m depth; red and blue colors depict *N. pachyderma* and *T. quinqueloba*, respectively. (a) Sea surface temperature and salinity and insolation at the top of the atmosphere; legend is the same as Figure 4. (b) Here $\delta^{18}O$ of *N. pachyderma* and *T. quinqueloba* versus $\delta^{18}O_{eq}$. Note low values, especially during spring and summer, and reversed $\delta^{18}O$ axis. (c) Weekly averaged interspecies oxygen isotope contrast. (d) Weekly averaged shell fluxes of *N. pachyderma* and *T. quinqueloba*. Vertical dashed lines separate phases defined in text.

is most pronounced. The flux of BSi decreases to background values.

[19] 5. In mid-September–October, surface cooling weakens stratification until the upper water column is mixed at the end of October. All shell fluxes fall to background levels, but that of *T. quinqueloba* is sustained longest.

4.2. Oxygen Isotopes

[20] The temporal patterns of oxygen isotope values are very similar in both species (Figures 5, 6, and 7). Both show a seasonal amplitude of ~2‰ with highest values in early spring and lowest in autumn and winter (Figure 5a). Both species exhibit an increase of over 0.7‰ from winter, when export production almost ceased (phase 1), to spring when production is resumed during phase 2 (Figures 5a and 6). Oxygen isotopes of *N. pachyderma* vary between 0.9‰ and 2.6‰, i.e., with an amplitude comparable to that of surface $\delta^{18}O_{eq}$ (Figure 5a). Highest values occur when production starts in spring when SST is still low; a minimum is present around SST maximum during the start of autumn. Low isotope values are recorded again in late autumn/winter (Figure 5a), but since only very few shells could be measured for these low fluxes $\delta^{18}O$ values are less accurate than for the preceding phases. The oxygen isotope values for *T. quinqueloba* vary over a wider range, between 1.4‰ and 3.8‰. In 35 out of 37 cases they are higher than in *N. pachyderma* (Figure 5a). The seasonal pattern is similar to that of *N. pachyderma* ($r^2 = 0.7$, n = 45, $P < 0.001$; and 0.9, n = 25, $P < 0.001$ during the growing season; Figure 7), resulting in a relatively stable $\Delta\delta^{18}O$ of 0.7‰ ± 0.2‰ (Figure 6c) that is independent of SST and stratification

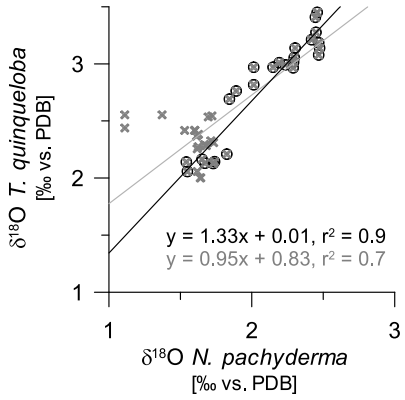

Figure 7. Scatterplot of weekly averaged oxygen isotope values of *N. pachyderma* and *T. quinqueloba*. Crosses depict values for the whole year. Open circles represent the period when fluxes of both species are above background values, i.e., when calcification takes place.

($r^2 = 0.2$, not shown). Like *N. pachyderma*, *T. quinqueloba* $\delta^{18}O$ shows a shift to lower values during late autumn/winter cooling. The spread within one sample is also considerably larger for *T. quinqueloba* (0.20‰ versus 0.07‰), probably due to the low shell mass with low gas yields that enhance the scatter in the measurements.

[21] The *N. pachyderma* $\delta^{18}O$ is lighter than surface $\delta^{18}O_{eq}$ when fluxes are low during phase 1 (Figure 6). As fluxes increase during spring bloom in phase 2, the offset from surface equilibrium disappears. Oxygen isotope values become progressively higher than surface equilibrium during phases 2 to 4 and remain relatively constant, crossing the surface equilibrium line, during phase 5 (Figure 6b). Values for *T. quinqueloba* are consistently larger than surface $\delta^{18}O_{eq}$ when export production is above background during phases 2 to 5 and even larger than $\delta^{18}O_{eq}$ at 200 m depth during phases 2 and 3 and most of phase 4 (Figure 6b). Both species show very similar temporal $\delta^{18}O$ patterns that primarily differ in their offset from surface equilibrium (Figures 6 and 7).

5. Discussion

[22] Time series shell fluxes show distinctly different patterns for *N. pachyderma* and *T. quinqueloba*. The flux of *N. pachyderma* starts earliest in the season and shows a bimodal pattern with one pulse in May and a second in early September. The flux of *T. quinqueloba*, on the other hand, starts later during the year, is clearly unimodal and reaches a maximum in September. Given their coherent temporal patterns and large amplitudes, the oxygen isotopes of both species closely trace a (near) surface signal rather than one at greater depth. The flux data thus suggest that differences in temporal habitat are more important in determining the sedimentary oxygen isotope signal than differences in the depth habitat of both species [cf. *Rashid and Boyle*, 2007; *Simstich et al.*, 2003]. In this section we will analyze the observed flux patterns and constrain the depth at which both species record temperature to propose a new way to infer past stratification differences.

5.1. Annual Flux Patterns

[23] All particle fluxes are lowest during winter and highest during summer (Figures 3 and 4). The shell flux patterns show a temporal structure different from seasonal SST, suggesting that they are not directly related. Moreover, elsewhere both species also thrive at lower temperatures than those reached in winter in the Irminger Sea when fluxes are virtually zero [*Bé and Tolderlund*, 1971]. Deep winter mixing [*Pickart et al.*, 2003; *Vage et al.*, 2009] and low insolation apparently limit primary production and ultimately cause the shell fluxes to be near zero in winter. Shell fluxes show two peaks during the year. The first peak occurs when the deep winter mixed layers starts to erode due to intermittent (re)stratification. The second peak arrives around the SST maximum when the upper water column is fully stratified. We therefore conclude that in the Irminger Sea not absolute temperature, but rather temperature differences, i.e., stratification and other factors such as light and food availability, control export shell fluxes.

[24] The rise in BSi flux during phase 2 marks the start of the spring bloom (Figure 4b), which is also evident from the increasing N and C_{org} fluxes (Figure 3d). Its timing agrees well with enhanced surface chlorophyll concentrations recorded by spaceborne sensors [*Henson et al.*, 2006; *Siegel et al.*, 2002]. The BSi flux appears to reach a broad maximum between the shell flux maxima of *N. pachyderma* and *T. quinqueloba* (Figure 4b). The flux of BSi, considered to reflect diatom export from the surface layer, reached values above background only when insolation exceeded a threshold (~275 W m^{-2} at the top of the atmosphere) during phases 2, 3 and 4. Together with BSi the flux of *N. pachyderma* starts to increase during the spring bloom (phase 2). With the onset of stable surface stratification, when SST increases rapidly (phase 3), the export flux of *N. pachyderma* decreases again (Figures 4b and 4c). The second flux pulse during phases 4 and 5 starts after BSi fluxes reached their maxima and peaks around SST maximum. The export flux of *N. pachyderma* is not directly related to permanent stratification, as it starts earlier and because its temporal pattern is bimodal. Such bimodality of the *N. pachyderma* flux might be caused by competition by other species in June and July (Figure 3c) that is overcome when growth conditions are optimal and all species fluxes peak at maximum SST and stratification. A double pulse in the flux of *N. pachyderma* (Figure 4c) is consistent with findings by *Tolderlund and Bé* [1971] in the North Atlantic, but was not found in the colder Arctic and Nordic Seas that are characterized by a single broad production period in summer [*Bauch et al.*, 1997; *Simstich et al.*, 2003; *Volkmann and Mensch*, 2001]. The relative contribution of the two seasonal pulses to the annual flux appears to be approximately equal (spring/autumn = 0.9), suggesting that the high *N. pachyderma* flux in July 2007 would be proportional to the following autumn pulse (Figure 3c).

[25] There is pronounced interannual variability in the *N. pachyderma* fluxes during phases 4 and 5 (Figure 4c). Using a Student's t test we evaluated whether the monthly shell fluxes during the minimum around the transition from phase 3 to phase 4 were significantly different from those during the months surrounding it. With a confidence level of alpha = 10% it is yet impossible to conclude that there is a significant difference in the mean of the monthly fluxes from April to September. However, such statistics are confounded by (1) the interannual differences in timing of the flux pulses, (2) the fact that the data represent intervals that spread beyond the month boundaries, and (3) the unequal temporal spacing of the data over the 3 year long record. Therefore, we stress the importance of the observation of a double pulse and the associated minimum in the annual flux of *N. pachyderma*. Although the present time series is too short to provide a statistically robust basis, we observe that bimodality characterizes the annual flux pattern of *N. pachyderma* in the Irminger Sea in our record. Such a bimodal flux agrees with temporal abundance data of the species in the North Atlantic [*Tolderlund and Bé*, 1971]. Finally and importantly, the statistics should not distract from the fact that the *N. pachyderma* export flux clearly starts earlier in the year than that of *T. quinqueloba*.

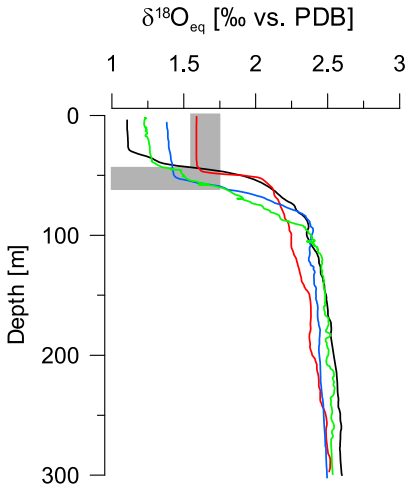

Figure 8. *N. pachyderma* $\delta^{18}O$ with respect to $\delta^{18}O_{eq}$ of the upper 300 m. The $\delta^{18}O_{eq}$ values are based on CTD casts (legend in Figure 2). Gray bars highlight *N. pachyderma* $\delta^{18}O$ at same time during the year as the CTD casts. Since *N. pachyderma* reflects $\delta^{18}O_w$ without a significant offset from equilibrium (see Figure 6c, phases 2 and 5), its oxygen isotope signal reflects $\delta^{18}O_w$ at or just below the base of the surface mixed layer.

[26] The unimodal flux pattern of *T. quinqueloba* (Figure 4d) suggests that this species is more uniformly driven by seasonal variations in stratification than *N. pachyderma*. Repeated plankton tows further south in the North Atlantic [*Tolderlund and Bé*, 1971] revealed a bimodal abundance pattern for *T. quinqueloba* whereas a unimodal flux pattern is a common feature at higher-latitude localities [*Schröder-Ritzrau et al.*, 2001; *Simstich et al.*, 2003]. The unimodal flux pattern of *T. quinqueloba* suggests that the species is in the colder part of its temperature range in the Irminger Sea. The observation that the flux of *T. quinqueloba* is sustained further into the cold season than *N. pachyderma* (Figure 4d, phase 5) might be due to the presence of symbionts [*Hemleben et al.*, 1989] that would allow *T. quinqueloba* to persist when food availability declines.

[27] Seasonal differences in shell fluxes cause the flux-weighted $\delta^{18}O$ of both species to represent temperature during different times of the year. Thus *N. pachyderma* reflects an average of near minimum and maximum temperature, whereas *T. quinqueloba* dominantly reflects the latter. The similarity in the amplitude and pattern of $\delta^{18}O$ of both species *N. pachyderma* and *T. quinqueloba* can only be explained by variations in the upper ocean and not by temperature changes at greater depths. Therefore, the seasonal shell flux variability and not interspecies depth habitat differences, dominantly determines the sedimentary $\Delta\delta^{18}O$ signal.

5.2. Shell $\delta^{18}O$: Temperature at What Depth?

[28] Since annual surface salinity variability is small compared to temperature changes, shell $\delta^{18}O$ will dominantly register temperature. The hydrographic data allow us to derive the depth at which the shell $\delta^{18}O$ reflects temperature. This depth is not necessarily equal to the depth habitat of the species involved as the foraminifera migrate through the upper water column while they build their skeleton [e.g., *Hemleben et al.*, 1989; *Lončarić et al.*, 2006; *Peeters et al.*, 2002]. A species' $\delta^{18}O$ thus reflects a weighted average of seawater $\delta^{18}O$ of its depth range. For inference of past upper ocean dynamics it is imperative to constrain the depth at which the oxygen isotopes reflect temperature, rather than knowing the actual depth habitat of the living species. Seasonal changes in the salinity-$\delta^{18}O_w$ relationship due to meltwater input may potentially bias our depth inferences. However, the influence of salinity on $\delta^{18}O_{eq}$ is much smaller than that of temperature (0.12‰ versus 1.82‰). The effect of a constant salinity-$\delta^{18}O_w$ relationship is thus insignificant for the annual $\delta^{18}O_{eq}$ pattern and our depth estimates will not critically depend on the relationship used.

[29] The upper water column is well mixed during phase 2 and equilibrium $\delta^{18}O$ values are therefore effectively equal at all depths. This period thus allows for the determination of any species specific offset from $\delta^{18}O_{eq}$. During phase 2, *N. pachyderma* $\delta^{18}O$ approaches $\delta^{18}O_{eq}$ closely (Figure 6a), thus recording $\delta^{18}O_w$ and temperature without a significant offset from $\delta^{18}O_{eq}$. When the water column is stratified (phases 3 to 5) the isotopic offset from surface equilibrium increases, indicating that *N. pachyderma* traces temperature below the developing surface mixed layer. For a constant zero offset from $\delta^{18}O_{eq}$, the depth at which *N. pachyderma* $\delta^{18}O$ reflects temperature can be constrained with the CTD profiles to just below the isothermal surface mixed layer at approximately 50 m depth in summer (Figure 8). This is shallower than the 100–150 m calcification range reported previously [e.g., *Kozdon et al.*, 2009; *Peck et al.*, 2008; *Simstich et al.*, 2003] and in apparent contradiction with abundance and isotope data from plankton tows in the North Atlantic Ocean and Nordic Seas conducted in July and August [*Bauch et al.*, 1997; *Stangeew*, 2001; *Volkmann and Mensch*, 2001]. These contrasting observations can however be reconciled when *N. pachyderma* incorporates a significant part of its $\delta^{18}O$ signal in the upper water column before descending to export depths around 150 m. Contrary to the zero offset in the Irminger Sea, *N. pachyderma* in the Nordic Seas records temperature with an offset around −0.6‰ from $\delta^{18}O_{eq}$ [*Simstich et al.*, 2003]. During phase 1, the $\delta^{18}O$ of *N. pachyderma* values are lower than surface $\delta^{18}O_{eq}$ and similar anomalously low values are found for *T. quinqueloba* (Figure 6). These low values are within range of the $\delta^{18}O_{eq}$ of the preceding SST maximum, particularly when considering the poorly constrained error on the single aliquot measurements. Therefore, we attribute these low isotopic values to a noncalcifying late summer population survives into the winter, rather than advection of shells from much warmer and/or fresher water. The subsequent step of 0.7‰ in $\delta^{18}O$ observed for both species during phase 1 (Figure 6) marks the turnover from a dormant noncalcifying population to a vital calcifying population that seeds the subsequent blooming. Since export fluxes outside the bloom period amount to only a few percent of the total annual flux, these low $\delta^{18}O$ values are insignificant for the average annual $\delta^{18}O$ signal. Thus the $\delta^{18}O$ of *N. pachyderma*

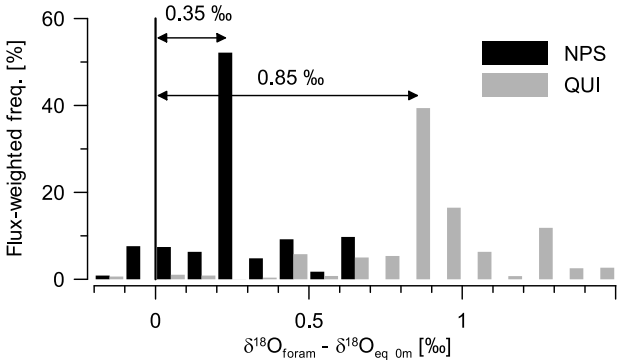

Figure 9. Flux-weighted frequency histogram of the species' offset from $\delta^{18}O_{eq}$ at the surface. Inclusion or exclusion of the period with extremely high fluxes of *N. pachyderma* in spring 2007 does not significantly alter the mean or modal offset.

accurately and dominantly reflects seawater temperature at the base of the surface mixed layer with a flux-weighted mean offset from surface $\delta^{18}O_{eq}$ of around +0.3‰ (Figure 9) equivalent to about −1.3°C.

[30] Oxygen isotope values of *T. quinqueloba* seem to reflect very low temperatures at face value, hence suggesting a much deeper habitat compared to *N. pachyderma* (Figures 3c and 6b). However, the expected isotope temperatures as calculated from the *Kim and O'Neil* [1997] equation would drop well below the observed 2.5°C at trap depth (2750 m). Furthermore, the amplitude in $\delta^{18}O$ indicates that *T. quinqueloba* experienced a seasonal temperature cycle that matches that of SST at the site as well as that of *N. pachyderma* from the same samples. Since the annual temperature amplitude at the site decreases with depth, the $\delta^{18}O$ of *T. quinqueloba* must reflect temperature at, or close to, the sea surface. This strongly provides evidence for an offset from equilibrium calcification, with a flux-weighted modal value of +0.85‰ with respect to surface $\delta^{18}O_{eq}$ (Figure 9). Period 2 offers again the possibility to deduce the offset from $\delta^{18}O_{eq}$ directly, since the water column is then completely mixed. Indeed, *T. quinqueloba* shows a +0.7‰ offset from $\delta^{18}O_{eq}$, which is consistent with the +0.85‰ offset from surface $\delta^{18}O_{eq}$ (Figure 6). The high correlation between the $\delta^{18}O$ of *N. pachyderma* and *T. quinqueloba* and the close to 1 slope of the regression line indicates that both species record temperature at approximately the same depth near the surface (Figure 7). We therefore conclude that in the Irminger Sea the $\delta^{18}O$ of *T. quinqueloba* reflects temperature at a similar near surface depth as *N. pachyderma*. However, in contrast to in the Nordic Seas, it does so with a significant positive offset from equilibrium [*Simstich et al.*, 2003]. Interestingly the $\delta^{18}O$ values of *T. quinqueloba* show an abrupt decrease in the offset from surface $\delta^{18}O_{eq}$ in phase 4, just prior to SST maximum (Figure 6b). This possibly indicates minor differences in calcification regimes or depths before and after the shift. The flux-weighted offset from surface $\delta^{18}O_{eq}$ (Figure 9) has however a clear mode at +0.85‰, indicating that the sedimentary $\delta^{18}O$ *T. quinqueloba* reflects $\delta^{18}O$ and temperature at the same depth as *N. pachyderma*, but with a greater offset from surface $\delta^{18}O_{eq}$.

[31] Both species thus record temperatures at or just below the seasonal SML; *N. pachyderma* with very little offset from $\delta^{18}O_{eq}$ and *T. quinqueloba* on average +0.7‰ heavier $\delta^{18}O_{eq}$ To the best of our knowledge only *Volkmann and Mensch* [2001] reported such a positive interspecies $\Delta\delta^{18}O$ in a high northern location, whereas others found isotopically lighter *T. quinqueloba* relative to *N. pachyderma* [e.g., *Castañeda et al.*, 2004; *Simstich et al.*, 2003; *Stangeew*, 2001]. To account for the observed $\Delta\delta^{18}O$, the local hydrography (Figures 1 and 2) offers little ground as the water column appears normally stratified. Advection of *T. quinqueloba* from a different water mass is unlikely given the remarkable similarity, in both timing and amplitude, between its $\delta^{18}O$ and the ambient $\delta^{18}O_{eq}$ pattern. To compensate for the 0.7‰ offset between the two species, *T. quinqueloba* would need to be advected from areas far south of the mooring site where $\delta^{18}O_w$ values are higher, or from within the East Greenland Current (EGC) where temperatures are much lower. However, in the first case advection is unlikely given the settling velocity of the shells that prevent their transport over such distances [cf. *Von Gyldenfeldt et al.*, 2000] and in the second case the $\delta^{18}O$ amplitude of *T. quinqueloba* would remain unexplained as seasonal temperature differences in the EGC are only in the order of 2°C–3°C. Advection of only the shells of *T. quinqueloba* is unlikely anyhow given the consistently high correlation between the $\delta^{18}O$ of *T. quinqueloba* and *N. pachyderma* throughout the 3 year time series (Figures 6 and 7). An alternative explanation for the contrasting $\Delta\delta^{18}O$ could be a difference in the species specific offset from equilibrium calcification between the Irminger Sea and the Nordic Seas [*Simstich et al.*, 2003]. Clearly, such a variable isotopic offset and interspecies contrast require further study as they may seriously affect reconstructions of past oceanographic change.

5.3. Seasonal Paleoceanography

[32] Since fluxes are nearly zero during the winter season when the water column is mixed to great depths, wintertime phenomena will not be directly reflected in the sedimentary record. Consequently, it is difficult to infer the past occurrence of deep convection in the Irminger Sea from planktonic foraminiferal proxies. Spring to autumn conditions, on the other hand, will dominate the sedimentary $\delta^{18}O$ signal, enabling inference of seasonal stratification changes. *Simstich et al.* [2003] proposed the use of the isotopic difference between *N. pachyderma* and *T. quinqueloba* as an indicator of stratification. They argued that in the Nordic Seas *N. pachyderma* records temperature deeper in the water column than *T. quinqueloba* and that therefore the interspecies $\Delta\delta^{18}O$ could be used to infer thermal stratification from sediment records. In the Irminger Sea however, the species seem to reflect temperature at the same depth, offering an alternative approach to infer past stratification that is based on flux timings rather than differences in depth habitat. Evidently, all such approaches depend critically on the assumption of a constant species specific offset from equilibrium calcification. This assumption may not always

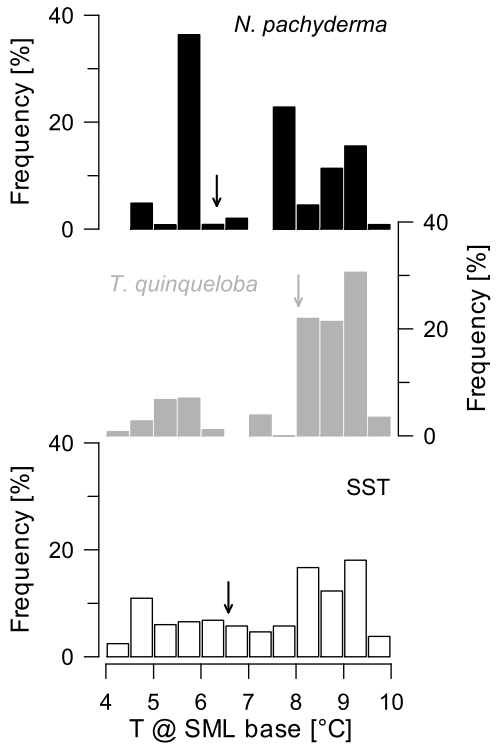

Figure 10. Flux-weighted temperature estimates based on $\delta^{18}O$ *N. pachyderma* and interspecies offset corrected *T. quinqueloba* compared to the temperature distribution of surface waters. Temperatures were calculated according to *Kim and O'Neil* [1997], ignoring $\delta^{18}O_w$ variability. The sedimentary $\delta^{18}O$ of both species will reflect temperature during different seasons, thus enabling inference of past seasonal temperature contrasts. Arrows indicate average values.

hold as our data suggest that regional differences in isotopic offsets occur.

[33] The data presented here offer two potential ways to assess past seasonal near surface temperature variability from sedimentary records. The first way is to use the bulk isotopic contrast between *T. quinqueloba* and *N. pachyderma*. Since the export flux of *T. quinqueloba* is concentrated in summer, its sedimentary $\delta^{18}O$ dominantly represents temperature maxima. The export flux of *N. pachyderma* however extends from early spring to late summer and the species $\delta^{18}O$ consequently reflects a weighted average of near minimum and maximum temperatures (Figure 10). Their isotopic difference thus reflects the seasonal thermal contrast at the base of the surface mixed layer and consequently an indicator for stratification. Smaller $\Delta\delta^{18}O$ values indicate decreased seasonality and vice versa. This approach requires that *N. pachyderma* records early spring and late summer temperatures, thus either a bimodal flux or a single broad production period through the year. Both are probably not the case when *N. pachyderma* dominates the sedimentary record, such as in colder conditions at higher latitudes where it only displays a narrow unimodal flux in late summer. Care should thus be taken when interpreting $\Delta\delta^{18}O$ changes across large temperature shifts. To derive an equation that links sedimentary $\Delta\delta^{18}O$ quantitatively to seasonal SST contrast, similar time series of shell fluxes across an SST gradient are required. Such studies may also reveal the mechanism causing the unimodal and bimodal flux patterns of planktonic foraminifera.

[34] As a second approach a bimodal flux pattern such as shown by *N. pachyderma* could be more optimally used for seasonal paleoceanography when individual shell isotope variability is considered. Potentially the two production periods during the year will result in a bimodal $\delta^{18}O$ frequency histogram, allowing direct inference of both maximum and near minimum temperature and consequently a conservative estimate of seasonality. Such a single specimen approach clearly offers great potential for the reconstruction of seasonal temperature and stratification variability.

6. Conclusions

[35] Multiyear time series of intercepted particle fluxes in the central Irminger Sea reveal the following.

[36] 1. Total mass and especially shell fluxes of *N. pachyderma* and *T. quinqueloba* are not primarily controlled by absolute seas surface temperatures, but rather by other factors such as seasonal stratification of the upper water column, insolation and food availability.

[37] 2. Production of *N. pachyderma* starts earliest in the season and shows one pulse in spring and a second around maximum stratification in late summer. The production of *T. quinqueloba* follows later during the season with a single peak around maximum stratification. It is continued longer during autumn/winter cooling.

[38] 3. The low fluxes during winter preclude the registration of wintertime phenomena such as deep convection, in sediments.

[39] 4. A dormant noncalcifying summer population of *N. pachyderma* and *T. quinqueloba* remains present in the water column during autumn and winter cooling. This population is replaced upon restratification of the water column during spring when shell fluxes rise.

[40] 5. The oxygen isotope signal of *N. pachyderma* reflects temperature at around 50 m, just below the base of the surface mixed layer when stratification is at its maximum. Oxygen isotope values of *T. quinqueloba* reflect temperature at the same depth but show a flux-weighted mean offset of about +0.7‰ with respect to equilibrium calcification.

[41] 6. Based on previous findings reported in literature, there are indications that the offset from equilibrium calcification of both species may vary regionally. This likely complicates paleoceanographic reconstructions based on the $\delta^{18}O$ of either *N. pachyderma* or *T. quinqueloba* or on their $\Delta\delta^{18}O$.

[42] 7. In the Irminger Sea both species record temperature around the same depth but during different periods of the year, the sedimentary isotopic contrast between *N. pachyderma* and *T. quinqueloba* may serve as an indicator of (changes in) past seasonality.

[43] **Acknowledgments.** We thank the captains and crew on board R/V *Pelagia* cruises 64PE216 and 64PE240, RRS *Discovery* cruise D309/10, and RRS *Charles Darwin* cruise CD164. Santiago Gonzalez, Karel Bakker, Evaline van Weerlee, Michiel Kienhuis, Sharyn Crayford, and Erica Koning are thanked for analytical support. The sediment trap lent to us through Richard Lampitt when ours failed at sea is greatly appreciated. We thank three anonymous reviewers for their constructive feedback on the manuscript. We acknowledge funding within the VAMOC (RAPID) program NWO grant 854.00.020 and through NWO middelgroot grant 34.07.001.

References

Aksu, A. E., R. N. Hiscott, M. A. Kaminski, P. J. Mudie, H. Gillespie, T. Abrajano, and D. Yasar (2002), Last glacial-Holocene paleoceanography of the Black Sea and Marmara Sea: Stable isotopic, foraminiferal and coccolith evidence, *Mar. Geol.*, *190*(1–2), 119–149, doi:10.1016/S0025-3227(02)00345-6.

Bacon, S., W. J. Gould, and Y. Jia (2003), Open-ocean convection in the Irminger Sea, *Geophys. Res. Lett.*, *30*(5), 1246, doi:10.1029/2002GL016271.

Bauch, D., J. Carstens, and G. Wefer (1997), Oxygen isotope composition of living *Neogloboquadrina pachyderma* (sin.) in the Arctic Ocean, *Earth Planet. Sci. Lett.*, *146*(1–2), 47–58, doi:10.1016/S0012-821X(96)00211-7.

Bauerfeind, E., and B. von Bodungen (2006), Underestimation of biogenic silicon flux due to dissolution in sediment trap samples, *Mar. Geol.*, *226*(3–4), 297–306, doi:10.1016/j.margeo.2005.11.001.

Bé, A. W. H., and D. S. Tolderlund (1971), Distribution and ecology of living planktonic foraminifera in surface waters of the Atlantic and Indian oceans, in *The Micropaleontology of Oceans*, edited by B. M. Funnell and W. R. Riedel, pp. 105–149, Cambridge Univ. Press, Cambridge, U. K.

Berger, A. L. (1978), Long-term variations of daily insolation and Quaternary climatic changes, *J. Atmos. Sci.*, *35*(12), 2362–2367, doi:10.1175/1520-0469(1978)035<2362:LTVODI>2.0.CO;2.

Bigg, G. R., and E. J. Rohling (2000), An oxygen isotope data set for marine water, *J. Geophys. Res.*, *105*, 8527–8535, doi:10.1029/2000JC900005.

Bonnin, J., W. van Raaphorst, G.-J. Brummer, H. van Haren, and H. Malschaert (2002), Intense mid-slope resuspension of particulate matter in the Faeroe-Shetland Channel: Short-term deployment of near-bottom sediment traps, *Deep Sea Res., Part I*, *49*(8), 1485–1505, doi:10.1016/S0967-0637(02)00030-4.

Carstens, J., D. Hebbeln, and G. Wefer (1997), Distribution of planktic foraminifera at the ice margin in the Arctic (Fram Strait), *Mar. Micropaleontol.*, *29*(3–4), 257–269, doi:10.1016/S0377-8398(96)00014-X.

Castañeda, I. S., L. M. Smith, G. B. Kristjánsdóttir, and J. T. Andrews (2004), Temporal changes in Holocene $\delta^{18}O$ records from the northwest and central North Iceland Shelf, *J. Quat. Sci.*, *19*(4), 321–334, doi:10.1002/jqs.841.

Cifelli, R. (1973), Observations on *Globigerina pachyderma* (Ehrenberg) and *Globigerina incompta* Cifelli from the North Atlantic, *J. Foraminiferal Res.*, *3*(4), 157–166, doi:10.2113/gsjfr.3.4.157.

Conan, S. M. H., and G. J. A. Brummer (2000), Fluxes of planktic foraminifera in response to monsoonal upwelling on the Somalia Basin margin, *Deep Sea Res., Part II*, *47*(9–11), 2207–2227, doi:10.1016/S0967-0645(00)00022-9.

Darling, K. F., M. Kucera, D. Kroon, and C. M. Wade (2006), A resolution for the coiling direction paradox in *Neogloboquadrina pachyderma*, *Paleoceanography*, *21*, PA2011, doi:10.1029/2005PA001189.

Deuser, W. G., and E. H. Ross (1989), Seasonally abundant planktonic foraminifera of the Sargasso Sea: Succession, deep-water fluxes, isotopic compositions, and paleoceanographic implications, *J. Foraminiferal Res.*, *19*(4), 268–293, doi:10.2113/gsjfr.19.4.268.

Falina, A., A. Sarafanov, and A. Sokov (2007), Variability and renewal of Labrador Sea water in the Irminger Basin in 1991–2004, *J. Geophys. Res.*, *112*, C01006, doi:10.1029/2005JC003348.

Hemleben, C., M. Spindler, and O. R. Anderson (1989), *Modern Planktonic Foraminifera*, Springer, New York.

Henson, S. A., R. Sanders, C. Holeton, and J. T. Allen (2006), Timing of nutrient depletion, diatom dominance and a lower-boundary estimate of export production for Irminger Basin, North Atlantic, *Mar. Ecol. Prog. Ser.*, *313*, 73–84, doi:10.3354/meps313073.

Hillaire-Marcel, C., and A. de Vernal (2008), Comment on "Mixed-layer deepening during Heinrich events: A multi-planktonic foraminiferal $\delta^{18}O$ approach, " *Science*, *320*(5880), 1161, doi:10.1126/science.1153316.

Hut, G. (1987), Consultants group meeting on stable isotope reference samples for geochemical and hydrological investigations, 42 pp., Int. At. Energy Agency, Vienna.

Kahn, M. I., T. Oba, and T.-L. Ku (1981), Paleotemperatures and the glacially induced changes in the oxygen-isotope composition of sea water during late Pleistocene and Holocene time in Tanner Basin, *Calif. Geol.*, *9*(10), 485–490.

Kim, S.-T., and J. R. O'Neil (1997), Equilibrium and nonequilibrium oxygen isotope effects in synthetic carbonates, *Geochim. Cosmochim. Acta*, *61*(16), 3461–3475, doi:10.1016/S0016-7037(97)00169-5.

King, A. L., and W. R. Howard (2005), $\delta^{18}O$ seasonality of planktonic foraminifera from Southern Ocean sediment traps: Latitudinal gradients and implications for paleoclimate reconstructions, *Mar. Micropaleontol.*, *56*(1–2), 1–24, doi:10.1016/j.marmicro.2005.02.008.

Koning, E., G.-J. Brummer, W. Van Raaphorst, J. Van Bennekom, W. Helder, and J. Van Iperen (1997), Settling, dissolution and burial of biogenic silica in the sediments off Somalia (northwestern Indian Ocean), *Deep Sea Res., Part II*, *44*(6–7), 1341–1360, doi:10.1016/S0967-0645(97)00018-0.

Koning, E., E. Epping, and W. Van Raaphorst (2002), Determining biogenic silica in marine samples by tracking silicate and aluminium concentrations in alkaline leaching solutions, *Aquat. Geochem.*, *8*(1), 37–67, doi:10.1023/A:1020318610178.

Kozdon, R., A. Eisenhauer, M. Weinelt, M. Y. Meland, and D. Nürnberg (2009), Reassessing Mg/Ca temperature calibrations of *Neogloboquadrina pachyderma* (sinistral) using paired $\delta^{44/40}Ca$ and Mg/Ca measurements, *Geochem. Geophys. Geosyst.*, *10*, Q03005, doi:10.1029/2008GC002169.

Locarnini, R. A., A. V. Mishonov, J. I. Antonov, T. P. Boyer, and H. E. Garcia (2006), *World Ocean Atlas 2005*, vol. 1, *Temperature*, *NOAA Atlas NESDIS*, vol. 61, edited by S. Levitus, 182 pp., NOAA, Silver Spring, Md.

Lončarić, N., F. J. C. Peeters, D. Kroon, and G.-J. A. Brummer (2006), Oxygen isotope ecology of recent planktic foraminifera at the central Walvis Ridge (SE Atlantic), *Paleoceanography*, *21*, PA3009, doi:10.1029/2005PA001207.

Mulitza, S., A. Duerkoop, W. Hale, G. Wefer, and H. S. Niebler (1997), Planktonic foraminifera as recorders of past surface-water stratification, *Geology*, *25*(4), 335–338, doi:10.1130/0091-7613(1997)025<0335:PFAROP>2.3.CO;2.

Nansen, F. (1912), Das bodenwasser und die abkühlung des meeres: Mit 12 abbildungen im text, *Int. Rev. Gesamten Hydrobiol. Hydrogr.*, *5*(1), 1–42, doi:10.1002/iroh.19120050102.

Nørgaard-Pedersen, N., N. Mikkelsen, and Y. Kristoffersen (2007), Arctic Ocean record of last two glacial-interglacial cycles off North Greenland/Ellesmere Island—Implications for glacial history, *Mar. Geol.*, *244*(1–4), 93–108, doi:10.1016/j.margeo.2007.06.008.

Operational Oceanography Group (2006), Global Temperature-Salinity Profile Programme, http://www.nodc.noaa.gov/GTSPP/, Natl. Oceanogr. Data Cent., Silver Spring, Md.

Peck, V. L., I. R. Hall, R. Zahn, and H. Elderfield (2008), Millennial-scale surface and subsurface paleothermometry from the northeast Atlantic, 55-8 ka BP, *Paleoceanography*, *23*, PA3221, doi:10.1029/2008PA001631.

Peeters, F. J. C., G.-J. A. Brummer, and G. Ganssen (2002), The effect of upwelling on the distribution and stable isotope composition of *Globigerina bulloides* and *Globigerinoides ruber* (planktic foraminifera) in modern surface waters of the NW Arabian Sea, *Global Planet. Change*, *34*(3–4), 269–291, doi:10.1016/S0921-8181(02)00120-0.

Pflaumann, U., J. Duprat, C. Pujol, and L. D. Labeyrie (1996), SIMMAX: A modern analog technique to deduce Atlantic sea surface temperatures from planktonic foraminifera in deep-sea sediments, *Paleoceanography*, *11*, 15–35, doi:10.1029/95PA01743.

Pickart, R. S., M. A. Spall, M. H. Ribergaard, G. W. K. Moore, and R. F. Milliff (2003), Deep convection in the Irminger Sea forced by the Greenland tip jet, *Nature*, *424*(6945), 152–156, doi:10.1038/nature01729.

Rashid, H., and E. A. Boyle (2007), Mixed-layer deepening during Heinrich events: A multi-planktonic foraminiferal $\delta^{18}O$ approach, *Science*, *318*(5849), 439–441, doi:10.1126/science.1146138.

Schiebel, R., and C. Hemleben (2000), Interannual variability of planktic foraminiferal populations and test flux in the eastern North Atlantic Ocean (JGOFS), *Deep Sea Res., Part II*, *47*(9–11), 1809–1852, doi:10.1016/S0967-0645(00)00008-4.

Schmidt, G. A. (1999), Forward modeling of carbonate proxy data from planktonic foraminif-

era using oxygen isotope tracers in a global ocean model, *Paleoceanography*, *14*, 482–497, doi:10.1029/1999PA900025.

Schröder-Ritzrau, A., H. Andruleit, S. Jensen, C. Samtleben, P. Schäfer, J. Matthiessen, H. C. Hass, A. Kohly, and J. Thiede (2001), Distribution, export and alteration of fossilizable plankton in the Nordic Seas, in *The Northern North Atlantic: A Changing Environment*, edited by P. Schäfer et al., pp. 81–104, Springer, Berlin.

Shackleton, N. (1967), Oxygen isotope analyses and Pleistocene temperatures re-assessed, *Nature*, *215*(5096), 15–17, doi:10.1038/215015a0.

Siegel, D. A., S. C. Doney, and J. A. Yoder (2002), The North Atlantic spring phytoplankton bloom and Sverdrup's critical depth hypothesis, *Science*, *296*(5568), 730–733, doi:10.1126/science.1069174.

Simstich, J., M. Sarnthein, and H. Erlenkeuser (2003), Paired $\delta^{18}O$ signals of *Neogloboquadrina pachyderma* (s) and *Turborotalita quinqueloba* show thermal stratification structure in Nordic Seas, *Mar. Micropaleontol.*, *48* (1–2), 107–125, doi:10.1016/S0377-8398(02)00165-2.

Stangeew, E. (2001), Distribution and isotopic composition of living planktonic foraminifera *N. pachyderma* (sinistral) and *T. quinqueloba* in the high latitude North Atlantic, Ph.D. dissertation, Math. -Naturwiss. Fak., Christian-Albrechts-Univ., Kiel, Germany.

Tolderlund, D. S., and A. W. H. Bé (1971), Seasonal distribution of planktonic foraminifera in the western North Atlantic, *Micropaleontology*, *17*(3), 297–329, doi:10.2307/1485143.

Vage, K., R. S. Pickart, V. Thierry, G. Reverdin, C. M. Lee, B. Petrie, T. A. Agnew, A. Wong, and M. H. Ribergaard (2009), Surprising return of deep convection to the subpolar North Atlantic Ocean in winter 2007–2008, *Nat. Geosci.*, *2*(1), 67–72, doi:10.1038/ngeo382.

van Kreveld, S., M. Sarnthein, H. Erlenkeuser, P. Grootes, S. Jung, M. J. Nadeau, U. Pflaumann, and A. Voelker (2000), Potential links between surging ice sheets, circulation changes, and the Dansgaard-Oeschger cycles in the Irminger Sea, 60-18 Kyr, *Paleoceanography*, *15*, 425–442, doi:10.1029/1999PA000464.

Volkmann, R., and M. Mensch (2001), Stable isotope composition ($\delta^{18}O$, $\delta^{13}C$) of living planktic foraminifers in the outer Laptev Sea and the Fram Strait, *Mar. Micropaleontol.*, *42*(3–4), 163–188, doi:10.1016/S0377-8398(01)00018-4.

Von Gyldenfeldt, A.-B., J. Carstens, and J. Meincke (2000), Estimation of the catchment area of a sediment trap by means of current meters and foraminiferal tests, *Deep Sea Res., Part II*, *47* (9–11), 1701–1717, doi:10.1016/S0967-0645(00)00004-7.

Yashayaev, I., M. Bersch, and H. M. van Aken (2007), Spreading of the Labrador Sea water to the Irminger and Iceland basins, *Geophys. Res. Lett.*, *34*, L10602, doi:10.1029/2006GL028999.

G.-J. A. Brummer and L. Jonkers, Department of Marine Geology, Royal Netherlands Institute for Sea Research, PO Box 59, NL-1790 AB Den Burg, Netherlands. (lukas.jonkers@nioz.nl)

M. F. De Jong and H. M. van Aken, Department of Physical Oceanography, Royal Netherlands Institute for Sea Research, PO Box 59, NL-1790 AB Den Burg, Netherlands.

F. J. C. Peeters, Section Marine Biogeology, Faculty of Earth and Life Sciences, Vrije University Amsterdam, De Boelelaan 1085, NL-1081 HV Amsterdam, Netherlands.